CMS Physics Analysis Summary

Contact: cms-pag-conveners-exotica@cern.ch 2017/03/22

Inclusive search for new particles decaying to displaced jets at $\sqrt{s} = 13$ TeV

The CMS Collaboration

Abstract

A search for long-lived particles was performed with data corresponding to an integrated luminosity of 2.6 fb^{-1} collected at a center-of-mass energy of 13 TeV by the CMS experiment in 2015. The analysis exploits two customized topological trigger algorithms and an offline displaced-jet tagging algorithm. The multiplicity of displaced jets is used to search for the presence of a signal with a proper lifetime between 1 mm and 1000 mm. Pair-produced long-lived decays to four jet final states, with cross sections larger than 1.2 fb are excluded for a proper lifetime of 50 mm. For pair-produced long-lived decays to two b quarks and two leptons with equal decay rates between lepton flavors, cross sections larger than 2.5 fb are excluded for proper lifetimes between 70 mm and 100 mm. As a mass exclusion bound, pair-produced long-lived R-parity violating top squarks lighter than $550 - 1130$ GeV are excluded depending on their lifetime and decay mode. This mass exclusion bound is currently the most stringent bound available for top squark proper lifetimes greater than 3 mm.

1 Introduction

The study of physics beyond the standard model (BSM) is one of the main objectives of the ATLAS and CMS experiments at the CERN LHC. With no signal observed so far, the ATLAS and CMS results put severe bounds on BSM theories. The majority of these searches focus on particles with proper lifetimes $c\tau_0 < 1\,\text{mm}$ and contain requirements on the physics objects that reject longer lived particle decays. This leaves open the possibility that light long-lived particles could be produced but remain undetected. In this note, we present an inclusive search for long-lived particles decaying to various combinations of jets and leptons. The analysis exploits the information originating from the CMS calorimeters to reconstruct jets and measure their energies. The information from reconstructed tracks, in particular the transverse impact parameter, is used to discriminate the displaced-jets signal from the background of ordinary multijet events. The analysis is performed on data collected with the CMS detector from proton-proton collisions at a center-of-mass energy $\sqrt{s} = 13\,\text{TeV}$ in 2015. The data set corresponds to an integrated luminosity of $2.6\,\text{fb}^{-1}$. Results for similar signatures at $\sqrt{s} = 8$ TeV have been reported by ATLAS [1, 2] and CMS [3].

This note is structured as follows: Section 2 describes the analyzed data samples and the Monte Carlo (MC) simulated events used to design the study and interpret the results. Section 3 describes the displaced-jet tagger and event selection. The data-driven background estimation are described Section 4. The systematic uncertainties are discussed in Section 5. Results are discussed in Section 6, where the interpretation in terms of benchmark BSM scenarios is given. A summary is presented in Section 7.

2 Datasets and simulated samples

Events are collected from two dedicated online selection algorithms, designed to identify events with displaced jets. Both triggers have a requirement on H_T which is computed as the scalar sum of the p_T of the jets in the event, considering only jets with $p_\text{T} > 40\,\text{GeV}$ and $|\eta| < 3.0$. The inclusive trigger algorithm accepts events with $H_\text{T} > 500\,\text{GeV}$ and at least two jets with $p_\text{T} > 40\,\text{GeV}$ and $|\eta| < 2.0$, with each jet having no more than two associated prompt tracks. Tracks are classified as prompt if their transverse impact parameter relative to the beam line, $IP^{2\text{D}}$, is less than 1 mm. The exclusive trigger algorithm requires $H_\text{T} > 350\,\text{GeV}$ and at least two jets with $p_\text{T} > 40\,\text{GeV}$, $|\eta| < 2.0$, no more than two associated prompt tracks, and at least one associated track with transverse impact parameter $IP^{2\text{D}} > 5\sigma_{IP^{2\text{D}}}$, where $\sigma_{IP^{2\text{D}}}$ is the uncertainty on $IP^{2\text{D}}$. Samples selected solely with large H_T are used to study the performance of the online selection algorithms.

Events are selected offline requiring at least two jets with $p_\text{T} > 60\,\text{GeV}$ and $|\eta| < 2.0$. Two classes of events are considered: (i) events passing the inclusive trigger algorithm and with $H_\text{T} > 650\,\text{GeV}$ and (ii) events passing the exclusive trigger algorithm and with $H_\text{T} > 450\,\text{GeV}$. Combining these two classes of events results in 786 002 unique events.

The main source of background events originates from multijet production. The properties of this background process are studied using a simulated multijet sample, generated with PYTHIA8 [4]. The NNPDF 2.3 [5] parton distribution functions (PDFs) are used to model the parton momentum distribution inside the colliding protons. The event simulation includes the effect of multiple proton-proton collisions in the same bunch crossing and in bunch crossings nearby in time, referred to as pileup. Simulated samples are reweighted to match the pileup profile observed in data.

The analysis is interpreted with a set of benchmark signal models. The **Jet-Jet** model predicts pair-produced long-lived scalar neutral particles X^0 [6], each decaying to a light quark-antiquark pair, where light refers to u, d, s, c, and b quark. The two scalars are produced through a $2 \to 2$ scattering process, mediated by a Z^* propagator. The decay rate to each flavor is the same. The resonance mass m_{X^0} and proper lifetime $c\tau_0$ are varied between 50 and 1500 GeV and between 1 and 2000 mm, respectively. The trigger efficiencies for $m_{X^0} = 300$ GeV and $c\tau_0 = 1, 30$, and 1000 mm are 30%, 81%, and 42%, respectively. The trigger efficiencies for $c\tau_0 =$ 30 mm and $m_X = 50, 100$, and 1000 GeV are 2%, 14%, and 92%, respectively.

The **B-Lepton** model contains pair-produced long-lived top squarks in R-parity violating models of supersymmetry [7]. Each top squark decays to one b quark and a lepton, with equal decay rates to each of the three lepton flavors. The resonance mass $m_{\tilde{t}}$ and proper lifetime $c\tau_0$ are varied between 300 and 1000 GeV and between 1 and 1000 mm, respectively. The trigger efficiencies for $m_{\tilde{t}} = 300$ GeV and $c\tau_0 = 1, 30$, and 1000 mm are 15%, 41%, and 23%, respectively. The trigger efficiencies for $c\tau_0 =$30 mm and $m_{\tilde{t}} = 500, 700$, and 1000 GeV are 64%, 71%, and 74%, respectively.

These models are also investigated with modified branching fractions. The **Light-Light** model is the Jet-Jet model excluding decays to b quarks (equal decays to lighter quarks) and the **B-Mu**, **B-Ele**, and **B-Tau** models are derived from the B-Lepton model with 100% branching fraction to muons, electrons, and taus, respectively. Leptonic tau decays are included in the **B-Tau** interpretation. All signal samples are generated with PYTHIA8, with the same configuration as for the multijet sample.

3 Event selection and inclusive displaced-jet tagger

Events contain multiple primary vertices (PVs) corresponding to pileup occurring in the same proton bunch crossing. A description of the PV reconstruction can be found in Ref. [8]. The displaced-jet identification variables utilize the primary vertex with the highest squared transverse momentum sum of the constituent tracks. The PV reconstruction employs Gaussian constraints on the reconstructed position based on the luminous region, which is evaluated from the reconstructed primary vertices in many events. The choice of primary vertex is found to have a negligible effect on the analysis.

The analysis utilizes a dedicated tagging algorithm to identify displaced jets. For each jet, the algorithm takes as input the reconstructed tracks within $\Delta R = \sqrt{(\Delta\eta)^2 + (\Delta\phi)^2} < 0.4$ of the jet. Only tracks with $p_T > 1$ GeV and passing loose tracking quality criteria are considered. Three variables are considered for each jet in the event.

The first variable quantifies how likely it is that the jet originates from a given PV. For a given jet, $\alpha_{\text{jet}}(\text{PV})$ is defined for each PV as

$$\alpha_{\text{jet}}(\text{PV}) = \frac{\sum_{\text{tracks}\in\text{PV}} p_T^{\text{tracks}}}{\sum_{\text{tracks}} p_T^{\text{tracks}}}, \tag{1}$$

where the sum in the denominator is over all tracks associated to the jet and the sum in the numerator is over just the subset of these tracks originating from the given PV. The tagging variable α_{max} is the largest value of $\alpha_{\text{jet(PV)}}$ for the jet.

The second variable quantifies the typical recoil angle of a given track in a jet from the flight direction of the long-lived candidate particle. For each track, Θ_{2D} is computed as the angle between the track $\vec{p_T} = (p_x, p_y)$ at the track's innermost hit and the vector connecting the

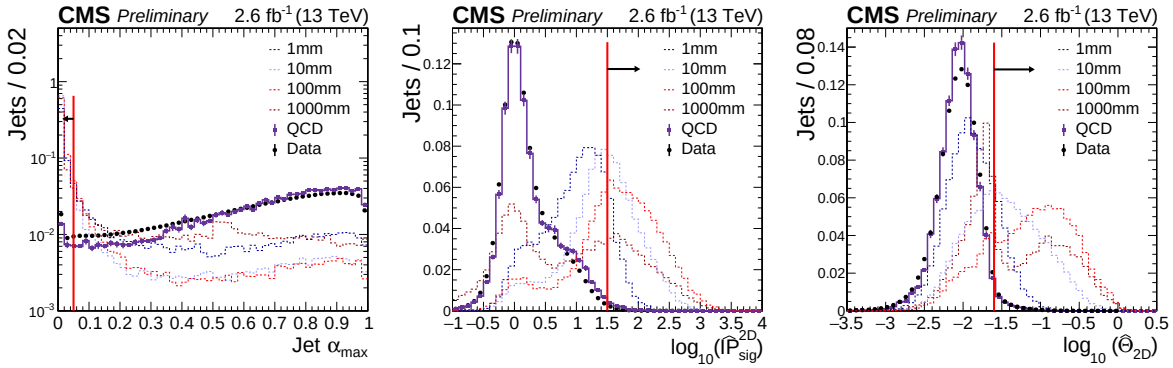

Figure 1: Comparison of MC and data distributions for the displaced-jet tagging variables α_{max} (left), $\widehat{IP}^{\text{2D}}_{\text{sig}}$ (center), and $\widehat{\Theta}_{\text{2D}}$ (right). The data distributions (circles) are compared to the expected background distributions from multijet events (squares) and several Jet-Jet benchmark models (dotted histograms) of pair-produced long-lived neutral scalar particles with $m_X = 700\,\text{GeV}$ and different values of $c\tau_0$. The vertical lines designate the value of requirement for the nominal displaced-jet tag. The direction of the arrow indicates the values included in the requirement. All distributions have unit normalization.

.

chosen PV to this hit in the transverse plane. The tagging variable $\widehat{\Theta}_{\text{2D}}$ is the median of the Θ_{2D} distribution for the tracks associated to the jet.

The third variable quantifies the significance of the measured transverse displacement for the jet. For each track associated to the jet, the significance of the track's transverse impact parameter, $IP^{\text{2D}}_{\text{sig}}$, is computed as the ratio of the track's transverse impact parameter and its uncertainty. The tagging variable $\widehat{IP}^{\text{2D}}_{\text{sig}}$ is the median of the $IP^{\text{2D}}_{\text{sig}}$ distribution of all tracks in a jet.

Figure 1 shows the distributions of the three tagging variables for data events, simulated multijet events, and simulated signal events with $m_{X^0} = 700\,\text{GeV}$ and several values of $c\tau_0$.

The displaced-jet identification criterion is $\alpha_{\text{max}} < 0.05$, $\log_{10}(\widehat{IP}^{\text{2D}}_{\text{sig}}) > 1.5$, and $\log_{10}(\widehat{\Theta}_{\text{2D}}) > -1.6$. This selection was chosen by scanning through the tagging variable parameter space and selecting parameters that yielded the best discovery significance for the Jet-Jet model across all generated lifetimes and masses.

The average displaced-jet tagging efficiency for $m_{X^0} = 700\,\text{GeV}$ is 4% for $c\tau_0 = 1\,\text{mm}$, 57% for $c\tau_0 = 30\,\text{mm}$, and 33% for $c\tau_0 = 1000\,\text{mm}$. For $c\tau_0 > 1000\,\text{mm}$, the long-lived particles typically decay beyond the tracker. For $c\tau_0 < 3\,\text{mm}$, the experimental signature for signal events becomes more similar to background b jets that decay in the tail of the lifetime distribution of B mesons.

A signal is searched for by applying the selection described above and counting the number of tagged displaced jets, N_{tags}. In addition to the online and offline requirements described in Section 2, the analysis signal region requires $N_{\text{tags}} \geq 2$. Efficiencies are reported for all interpreted models as a function of the lifetime with fixed mass (Tables 1 and 2) as well as a function of mass with fixed lifetime (Tables 3 and 4).

Table 1: Signal efficiencies (in %) for $m_{\chi^0} = m_{\tilde{t}} = 300\,\text{GeV}$ and varied $c\tau_0$ for the Jet-Jet and B-Lepton models. Selection requirements are cumulative from the first to the last row.

Jet-Jet

m_{χ^0} [GeV]	300	300	300	300
$c\tau_0$ [mm]	1	10	100	1000
≥ 2 tags	2.33 ± 0.15	39.49 ± 0.63	54.54 ± 0.74	14.58 ± 0.38
Trigger	2.16 ± 0.15	38.12 ± 0.62	39.32 ± 0.63	8.07 ± 0.28
Selection	2.09 ± 0.14	37.09 ± 0.61	36.53 ± 0.60	6.67 ± 0.26
≥ 3 tags	0.17 ± 0.04	14.14 ± 0.38	16.72 ± 0.41	1.36 ± 0.12
≥ 4 tags	0.01 ± 0.01	4.73 ± 0.22	4.71 ± 0.22	0.17 ± 0.04

B-Lepton

$m_{\tilde{t}}$ [GeV]	300	300	300	300
$c\tau_0$ [mm]	1	10	100	1000
≥ 2 tags	0.45 ± 0.02	15.82 ± 0.13	31.52 ± 0.19	8.55 ± 0.10
Trigger	0.29 ± 0.02	11.45 ± 0.11	17.08 ± 0.14	3.22 ± 0.06
Selection	0.27 ± 0.02	9.91 ± 0.11	13.33 ± 0.12	2.08 ± 0.05
≥ 3 tags	0.02 ± 0.01	2.46 ± 0.05	3.81 ± 0.07	0.37 ± 0.02
≥ 4 tags	–	0.30 ± 0.02	0.48 ± 0.02	0.03 ± 0.01

4 Background prediction

Background events arise from jets in which one or more displaced tracks are present due to either mismeasured tracks or truly displaced tracks such as from a weak decay of a strange, charm, or bottom hadron. As the proportion of tracks identified as being displaced is small and approximately constant, and two tagging variables use medians of all tracks associated with the jet, the likelihood of tagging a non-displaced jet as a displaced jet decreases exponentially with N_{tracks}. Figure 2 shows the fraction of jets that are tagged as displaced jets in data as a function of the number of tracks associated with the jet N_{tracks}. This function is the misidentification rate of tagging a prompt jet as displaced (assuming no signal contamination) and is interpreted as the probability $p(N_{\text{tracks}})$ of being tagged. This parameterization allows for an estimation, event by event, of the probability of tagging displaced jets.

To maintain the statistical independence of the events that are used to perform the prediction and the events in the signal region, the misidentification rate is measured in a control sample defined as events with $N_{\text{tags}} \leq 1$ (as shown in Figure 2), while the signal region requires $N_{\text{tags}} \geq 2$. Additionally, this limits signal contamination in the misidentification rate. There are 1391 events with $N_{\text{tags}} = 1$. The size of the bias introduced by only measuring the misidentification rate in events with $N_{\text{tags}} \leq 1$ is quantifiable. For the nominal tag requirement, the effect of removing events with $N_{\text{tags}} > 1$ on the predicted number of two tag events is negligible (0.4%) compared to the statistical uncertainty of the prediction.

The misidentification rate is used to predict the probability for an event to have N_{tags} tagged jets, $P(N_{\text{tags}})$. For instance, for an event m with three jets j_1, j_2, and j_3, there is one configuration with no tags, with a probability:

$$P^m(N_{\text{tags}} = 0) = (1 - p_1)(1 - p_2)(1 - p_3)\,,$$

where $p_i = p(N_{\text{tracks}}(j_i))$. Similarly, there are three configurtions for this same event to have

Table 2: Signal efficiencies (in %) for $m_{X^0} = m_{\tilde{t}} = 300\,\text{GeV}$ and varied $c\tau_0$ with modified branching ratios relative to the Jet-Jet and B-Lepton models. Selection requirements are cumulative from the first to the last row.

Light-Light				
m_{X^0} [GeV]	300	300	300	300
$c\tau_0$ [mm]	1	10	100	1000
≥ 2 tags	2.20 ± 0.19	40.49 ± 0.80	54.92 ± 0.93	14.55 ± 0.47
Trigger	2.04 ± 0.18	39.16 ± 0.78	39.63 ± 0.79	8.20 ± 0.36
Selection	2.03 ± 0.18	38.41 ± 0.77	36.99 ± 0.76	6.89 ± 0.33
≥ 3 tags	0.19 ± 0.05	14.77 ± 0.48	16.70 ± 0.51	1.48 ± 0.15
≥ 4 tags	–	5.11 ± 0.28	4.73 ± 0.27	0.22 ± 0.06
B-Ele				
$m_{\tilde{t}}$ [GeV]	300	300	300	300
$c\tau_0$ [mm]	1	10	100	1000
≥ 2 tags	0.81 ± 0.10	20.51 ± 0.47	39.01 ± 0.65	11.46 ± 0.35
Trigger	0.40 ± 0.07	14.68 ± 0.40	22.95 ± 0.50	5.15 ± 0.23
Selection	0.40 ± 0.07	13.92 ± 0.39	20.34 ± 0.47	3.58 ± 0.19
≥ 3 tags	0.04 ± 0.02	4.22 ± 0.21	7.21 ± 0.28	0.82 ± 0.09
≥ 4 tags	–	0.73 ± 0.09	1.19 ± 0.11	0.05 ± 0.02
B-Tau				
$m_{\tilde{t}}$ [GeV]	300	300	300	300
$c\tau_0$ [mm]	1	10	100	1000
≥ 2 tags	0.48 ± 0.07	18.40 ± 0.45	34.98 ± 0.61	9.31 ± 0.32
Trigger	0.44 ± 0.07	14.63 ± 0.40	20.20 ± 0.46	3.81 ± 0.20
Selection	0.41 ± 0.07	12.45 ± 0.37	15.50 ± 0.41	2.37 ± 0.16
≥ 3 tags	0.02 ± 0.02	3.23 ± 0.19	4.62 ± 0.22	0.44 ± 0.07
≥ 4 tags	–	0.53 ± 0.08	0.66 ± 0.09	0.02 ± 0.02
B-Mu				
$m_{\tilde{t}}$ [GeV]	300	300	300	300
$c\tau_0$ [mm]	1	10	100	1000
≥ 2 tags	0.13 ± 0.04	8.02 ± 0.29	20.09 ± 0.46	4.03 ± 0.21
Trigger	0.05 ± 0.02	3.97 ± 0.21	6.63 ± 0.26	0.88 ± 0.10
Selection	0.04 ± 0.02	2.92 ± 0.18	4.21 ± 0.21	0.49 ± 0.07
≥ 3 tags	–	0.23 ± 0.05	0.31 ± 0.06	0.03 ± 0.020
≥ 4 tags	–	0.01 ± 0.01	–	–

$N_{\text{tags}} = 1$:

$$P^m(N_{\text{tags}} = 1) = p_1(1-p_2)(1-p_3) + (1-p_1)p_2(1-p_3) + (1-p_1)(1-p_2)p_3\,.$$

The probability of finding N_{tags} tags in the m event is:

$$P^m(N_{\text{tags}}) = \sum_{\text{jet-configs}} \prod_{i \in \text{tagged}} p_i \prod_{k \in \text{not-tagged}} (1-p_k)\,. \tag{2}$$

Tagged jets enter the product as p_i and non-tagged jets enter as $(1-p_i)$. Equation (2) is used to compute the probability of observing N_{tags}, under the assumption that the sample does not contain any signal. The number of events expected for a given value of N_{tags} is computed as

$$N_{\text{events}}(N_{\text{tags}}) = \sum_m P^m(N_{\text{tags}})\,, \tag{3}$$

Table 3: Signal efficiencies (in %) for the Jet-Jet and B-Lepton models with $c\tau_0 = 30$ mm and varied mass. Selection requirements are cumulative from the first to the last row.

Jet-Jet

m_{X^0} [GeV]	50	100	300	1000	1500
$c\tau_0$ [mm]	30	30	30	30	30
≥ 2 tags	2.71 ± 0.10	14.80 ± 0.22	54.24 ± 0.74	79.93 ± 0.89	82.55 ± 0.91
Trigger	0.50 ± 0.04	5.39 ± 0.13	46.41 ± 0.68	74.05 ± 0.86	77.65 ± 0.88
Selection	0.30 ± 0.03	3.70 ± 0.11	44.75 ± 0.67	73.99 ± 0.86	77.53 ± 0.88
≥ 3 tags	0.05 ± 0.01	1.09 ± 0.10	20.87 ± 0.46	49.42 ± 0.70	55.28 ± 0.74
≥ 4 tags	–	0.22 ± 0.03	6.81 ± 0.26	25.45 ± 0.50	32.26 ± 0.57

B-Lepton

$m_{\tilde{t}}$ [GeV]	300	600	800	1000
$c\tau_0$ [mm]	30	30	30	30
≥ 2 tags	31.52 ± 0.19	47.32 ± 0.23	52.53 ± 0.24	55.88 ± 0.35
Trigger	17.08 ± 0.14	35.03 ± 0.20	40.40 ± 0.21	43.14 ± 0.30
Selection	14.70 ± 0.13	32.34 ± 0.19	36.94 ± 0.20	39.26 ± 0.29
≥ 3 tags	4.11 ± 0.07	10.76 ± 0.11	13.29 ± 0.12	15.00 ± 0.18
≥ 4 tags	0.55 ± 0.03	1.83 ± 0.05	2.69 ± 0.05	3.09 ± 0.08

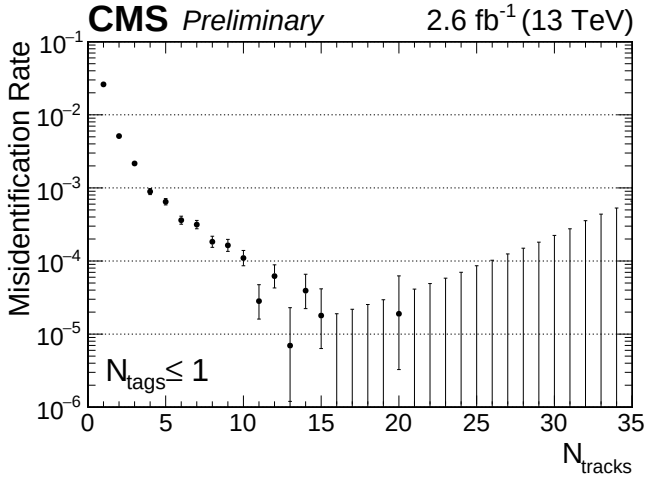

Figure 2: The fraction of jets passing the displaced-jet tagging criteria as a function of the number tracks associated with the jet. The results are from data events with $N_{\text{tags}} \leq 1$ collected with the displaced-jet triggers and passing the offline selection criteria.

where m runs only over events with fewer than two tagged jets. The prediction is then compared to the observed N_{tags} multiplicity in events with two or more tagged jets, to assess the presence of a signal.

We validate this procedure in the absence (background-only test) and presence (signal-injection test) of a signal, using simulated events.

The background-only test is performed by predicting the tag multiplicity on the simulated multijet sample, taking as input the misidentification rate distribution. In order to populate the large-N_{tags} region of the distribution, a looser version of the displaced-jet tagger is employed in this test. The full sample of events passing the event selection is divided into multiple in-

Table 4: Signal efficiencies (in %) for $c\tau_0 = 30$ mm and varied mass with modified branching ratios relative to the Jet-Jet and B-Lepton models. Selection requirements are cumulative from the first to the last row.

Light-Light

m_{X^0} [GeV]	50	100	300	1000	1500
$c\tau_0$ [mm]	30	30	30	30	30
≥ 2 tags	2.84 ± 0.12	15.56 ± 0.29	54.87 ± 0.92	80.52 ± 1.11	82.19 ± 1.14
Trigger	0.53 ± 0.05	5.70 ± 0.17	47.14 ± 0.85	74.85 ± 1.07	77.07 ± 1.10
Selection	0.33 ± 0.04	3.90 ± 0.14	45.68 ± 0.84	74.80 ± 1.07	76.96 ± 1.10
≥ 3 tags	0.05 ± 0.02	1.11 ± 0.08	21.77 ± 0.58	50.04 ± 0.88	55.36 ± 0.93
≥ 4 tags	–	0.23 ± 0.04	7.38 ± 0.34	25.80 ± 0.63	32.47 ± 0.71

B-Ele

$m_{\tilde{t}}$ [GeV]	300	600	800	1000
$c\tau_0$ [mm]	30	30	30	30
≥ 2 tags	39.01 ± 0.65	53.70 ± 0.75	59.62 ± 0.78	62.42 ± 1.11
Trigger	22.95 ± 0.50	38.07 ± 0.63	43.06 ± 0.66	45.21 ± 0.95
Selection	21.59 ± 0.48	37.02 ± 0.62	39.47 ± 0.64	42.20 ± 0.92
≥ 3 tags	7.86 ± 0.29	14.28 ± 0.38	17.37 ± 0.42	20.39 ± 0.64
≥ 4 tags	1.37 ± 0.12	3.32 ± 0.19	4.34 ± 0.21	4.69 ± 0.31

B-Tau

$m_{\tilde{t}}$ [GeV]	300	600	800	1000
$c\tau_0$ [mm]	30	30	30	30
≥ 2 tags	34.98 ± 0.61	51.42 ± 0.73	57.20 ± 0.76	59.43 ± 1.07
Trigger	20.20 ± 0.46	39.78 ± 0.64	45.46 ± 0.68	47.62 ± 0.96
Selection	17.17 ± 0.43	37.47 ± 0.62	43.64 ± 0.67	44.26 ± 0.92
≥ 3 tags	5.21 ± 0.24	13.29 ± 0.37	16.15 ± 0.40	19.13 ± 0.61
≥ 4 tags	0.86 ± 0.10	3.09 ± 0.18	3.68 ± 0.19	4.48 ± 0.29

B-Mu

$m_{\tilde{t}}$ [GeV]	300	600	800	1000
$c\tau_0$ [mm]	30	30	30	30
≥ 2 tags	20.09 ± 0.46	35.46 ± 0.60	41.18 ± 0.64	43.13 ± 0.93
Trigger	6.63 ± 0.26	24.73 ± 0.50	31.85 ± 0.56	34.10 ± 0.82
Selection	5.25 ± 0.24	21.40 ± 0.47	27.42 ± 0.52	31.18 ± 0.79
≥ 3 tags	0.34 ± 0.06	3.03 ± 0.18	5.28 ± 0.23	6.08 ± 0.35
≥ 4 tags	–	0.12 ± 0.04	0.68 ± 0.08	0.68 ± 0.12

dependent samples and the background prediction validated. The predicted background of N_{tags} events in simulated multijet events is found to be consistent with the observed number of events.

The signal-injection test is performed by adding events of pair-produced resonances decaying to two jets to the multijet sample and repeating the procedure described above. In this case, the nominal displaced-jet tagger is used. The injected signal has $m_{X^0} = 700\,\text{GeV}$ and $c\tau_0 = 10\,\text{mm}$ with a varied cross section. The jet probability is computed as in the data, where no prior knowledge of the nature of the events (signal or background) is available. In this case, the misidentification rate is derived from the mixed sample itself, including the contamination from the injected signal sample. The signal contamination is found to have a minimal impact

on the predicted number of events in the signal region. For example, with an injection cross section of 30 fb, 19 events are observed with two tags, while the 2 tag prediction is consistent with the predictions obtained for zero injected events: $N_{\text{events}}(N_{\text{tags}} \geq 2) = 1.3$. For example, with an injection cross section of 3 pb, no three tag events are predicted, while 1520 events with three tags are observed. Given the insensitivity of the predicted background to large amounts of injected signal, the analysis is robust to signal contamination.

5 Systematic uncertainties

5.1 Background systematic uncertainties

A background systematic uncertainty is determined for the data-driven background-prediction method. This uncertainty is estimated by repeating the background-prediction procedure described in Section 4 using a looser version of the displaced-jet tagging algorithm and comparing the predicted and observed number of events in data. The background estimation uncertainty of 7.5% is the required adjustment to the prediction to remove the observed bias. For three or more tags, the systematic uncertainty for the method is kept fixed.

The statistical uncertainty on the measured misidentification rate as a function of N_{tracks} is propagated to the predicted N_{tags} distribution as a systematic uncertainty. This systematic uncertainty is calculated for each tag multiplicity bin. The uncertainty for the 2 tag bin is 13%.

5.2 Signal systematic uncertainties

All signal systematic uncertainties are calculated individually for each model, for each mass and lifetime point, and for each value of N_{tags} in the signal region. In cases where the uncertainty depends on the mass, lifetime, and/or decay mode of the long-lived particle, a range is quoted, referring to the uncertainty for $N_{\text{tags}} = 2$ events. A summary of systematic uncertainties associated with the signal is given in Table 5.

The uncertainty on the trigger emulation is measured by comparing the predicted efficiency for simulated multijet events and data collected by a loose H_{T} trigger. The observed difference at threshold (5%) is taken as an estimate of the uncertainty in the emulation of the online H_{T} requirement. Similarly, the uncertainty induced by the online versus offline jet acceptance is obtained from the shift in the trigger efficiency when the offline jet p_{T} requirement is increased from $p_{\text{T}} > 60\,\text{GeV}$ to $p_{\text{T}} > 80\,\text{GeV}$ (5%).

The systematic uncertainty on the modeling of the online tracking efficiency is obtained by studying the online regional track reconstruction in data and MC. The online values of IP^{2D} and $IP^{\text{2D}}_{\text{sig}}$ are varied by the magnitude of the mismodeling found in events collected in control triggers. The new values are used to determine if the event would still pass at least one of the trigger paths and its associated offline H_{T} requirement. The N_{tags} distribution is recalculated with the values varied up and down. The relative change in the number of events per bin is taken as the systematic uncertainty. For $N_{\text{tags}} = 2$, this uncertainty varies from 1 to 35%.

The systematic uncertainty on the luminosity is 2.3% [9].

The uncertainty arising from the PDFs for pair-produced masses in the range of 50–1500 GeV is found to be 1–6%. An ensemble of alternative PDFs is sampled from the output of the NNPDF fit. Events are reweighted according to the ratio between these alternative PDF sets and the nominal ones. The distribution of the signal prediction for these PDF ensembles is used to quantify the uncertainty.

Table 5: Summary of the signal systematic uncertainties. When the uncertainty depends on the specific features of the models (mass, lifetime and decay mode of the long-lived particle) a range is quoted, which refers to the computed uncertainty for $N_{\text{tags}} = 2$ events.

Signal systematic uncertainty	**Effect on yield**
H_{T} trigger inefficiency	5%
Jet p_{T} trigger inefficiency	5%
Trigger online tracking modeling	1–35%
Luminosity	2.3%
Acceptance due to PDF	1–6%
Displaced-jet tag variable modeling	1–30%

Table 6: The predicted and observed number of events as a function of N_{tags}. The prediction is based on the misidentification rate derived from events with fewer than two tags. The full event selection is applied. The uncertainty corresponds to the total background systematic uncertainty.

N_{tags}	**Expected**	**Observed**
2	1.09 ± 0.16	1
≥ 3	$(4.9 \pm 1.0) \times 10^{-4}$	0

The systematic uncertainty on the modeling of the jet tagging variables in signal MC samples is estimated from the displaced track modeling in multijet events in data and MC. The mismodeling of the measured value of Θ_{2D} and $IP^{\text{2D}}_{\text{sig}}$ for single tracks is propagated to the final tag distribution by varying the individual measured values in MC by the difference in the measured value relative to data (3–10%). The tagging variables are then recalculated. The N_{tags} distribution is recalculated with the new values. The systematic uncertainty is assigned as the relative change in events, bin by bin in N_{tags}. For the two tag bin, this varies from 1 to 30% depending on the mass and lifetime. The mismodeling of α_{max} is found to have a negligible effect on the signal efficiency as the requirement is relatively loose.

6 Results and interpretation

The numerical values for the expected and observed yields are summarized in Table 6. The observed yields are found to be consistent with the predicted background, within the statistical and systematic uncertainties. No evidence for a signal at large values of N_{tags} is observed.

Exclusions for each model are obtained from the predicted and observed event yields in Table 6 and the signal efficiencies in Tables 1–4. All bounds are derived at 95% confidence-level (CL) according to the CL_s prescription [10–12] in the asymptotic approximation. For each limit derivation, we consider events with $N_{\text{tags}} \geq 2$ using independent bins for $N_{\text{tags}} = 2$ and $N_{\text{tags}} \geq 3$. Finer binning of the tag multiplicity for $N_{\text{tags}} > 3$ is found to have a negligible effect on the expected limits. Cross section upper limits are presented as a function of the mass and lifetime of the parent particle. The analysis sensitivity is maximal for $(10 < c\tau_0 < 1000)$ mm. Mass exclusion bounds at fixed lifetime are also derived, comparing the excluded cross section with the values predicted for the benchmark models described in Section 2. In the case of SUSY models, the next-to-leading order (NLO) and next-to-leading-logs (NLL) $\widetilde{\text{tt}}^*$ production cross section is used as a reference, computed in the large-mass limit for all other SUSY particles [13–18].

Figures 3 and 4 show the excluded pair-production cross section for the Jet-Jet and Light-Light models, respectively. Cross sections as small as 1.2 fb are excluded for $c\tau_0 = 50\,\text{mm}$ for both models. Exclusion limits are also derived for resonances decaying to bℓ final states, as shown in Fig. 5. The sensitivity is similar to what is observed for the Jet-Jet model, although less stringent as additional jets give higher efficiency than additional leptons from both the tagging and triggering perspectives. Cross sections larger than 2.5 fb are excluded at 95% CL, for $c\tau_0$ in the range 70–100 mm, which corresponds to excluding parent masses below 1130 GeV.

Figures 6 and 7 show the exclusions for the B-Tau and B-Ele models, respectively. The two models have similar performance at high mass with slightly stronger limits for the B-Ele model at lower mass ($m_{\tilde{t}} = 300\,\text{GeV}$) and longer lifetime ($c\tau_0 > 10\,\text{mm}$). The highest mass excluded in the B-Ele (B-Tau) model is $m_{\tilde{t}} = 1145\ (1150)\,\text{GeV}$ at $c\tau_0 = 70\ (70)\,\text{mm}$, corresponding to a cross section of 2.31 (2.23) fb at 95% CL.

Figure 8 shows the exclusion for the B-Mu model. Since the analysis uses jets reconstructed from calorimetric deposits and the two muons have small or no associated calorimeter deposits, the signal reconstruction efficiency and displaced-jet multiplicity are smaller in this case. This results in a weaker exclusion bound. The highest mass excluded in the B-Mu model is $m_{\tilde{t}} = 1085\,\text{GeV}$ at $c\tau_0 = 70\,\text{mm}$, corresponding to a cross section upper limit of 3.5 fb at 95% CL.

7 Summary

A search for long-lived particles was performed with data corresponding to an integrated luminosity of $2.6\,\text{fb}^{-1}$ collected at a center-of-mass energy of 13 TeV by the CMS experiment in 2015. This is the first search made for long-lived decays to jet final states in 13 TeV data and the first search to demonstrate explicit sensitivity to long-lived decays to tau leptons. The analysis utilized two customized topological trigger algorithms and an offline displaced-jet tagging algorithm, with the multiplicity of displaced jets used to search for the presence of a signal. As no excess above the predicted background is found, upper limits are set at 95% confidence level on the production cross section for resonances decaying to two jets or to a lepton and b quark. The limits are calculated as a function of the mass and proper lifetime of the long-lived particles. For the jet-jet (bottom-lepton) decay mode, cross sections larger than 1.2 fb (2.5 fb) are excluded for proper lifetimes of 50 mm (70–100 mm). The cross section limits are also translated into mass exclusion bounds, using a calculation of the top squark production cross section as a reference. Pair-produced long-lived R-parity violating top squarks lighter than 550–1130 GeV are excluded, depending on their lifetime and decay mode. This mass exclusion bound is currently the most stringent bound available for top squark proper lifetimes greater than 3 mm.

References

[1] ATLAS Collaboration, "Search for long-lived, weakly interacting particles that decay to displaced hadronic jets in proton-proton collisions at $\sqrt{s} = 8$ TeV with the ATLAS detector", *Phys. Rev. D* **92** (2015) 012010, doi:10.1103/PhysRevD.92.012010, arXiv:1504.03634.

[2] ATLAS Collaboration, "Search for massive, long-lived particles using multitrack displaced vertices or displaced lepton pairs in pp collisions at $\sqrt{s}$ = 8 TeV with the ATLAS detector", *Phys. Rev. D* **92** (2015) 072004, doi:10.1103/PhysRevD.92.072004, arXiv:1504.05162.

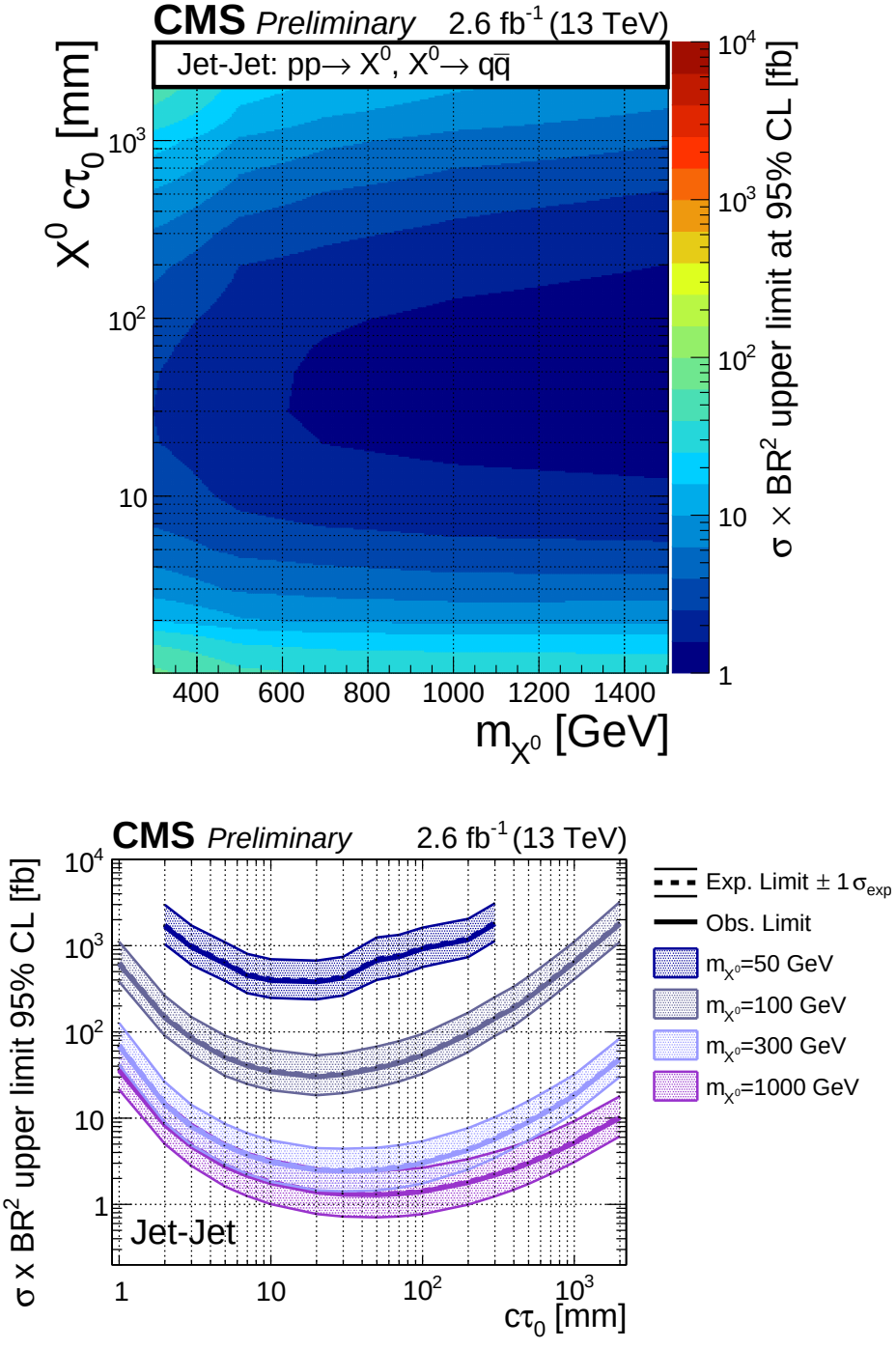

Figure 3: The excluded cross section at 95% CL for the Jet-Jet model as a function of the mass and proper lifetime of the parent particle X^0 (top) and as a function of the proper lifetime for four values of the mass (bottom). The bottom plot also shows the expected upper limits with one standard deviation uncertainties.

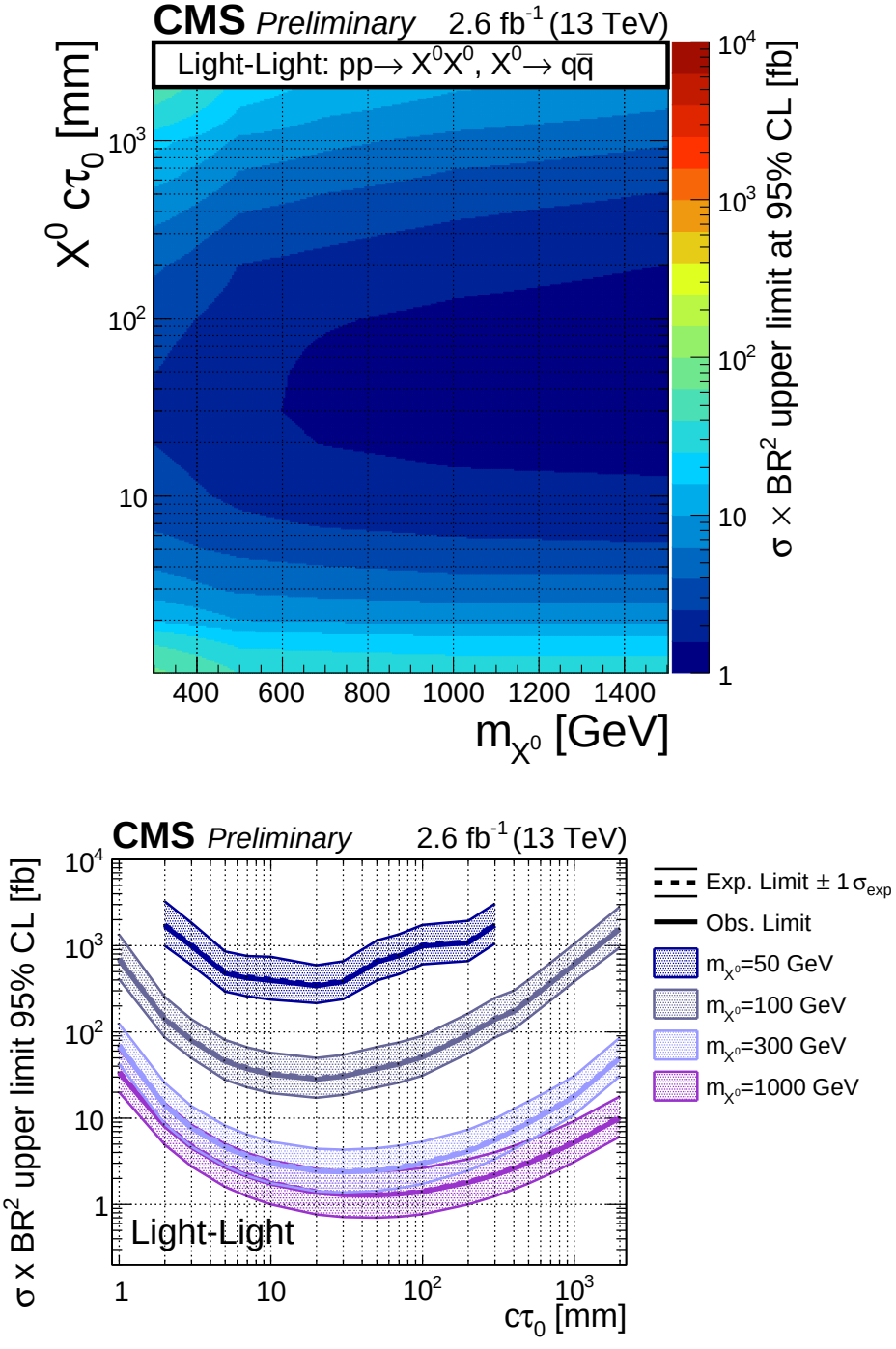

Figure 4: The excluded cross section at 95% CL for the Light-Light model as a function of the mass and proper lifetime of the parent particle X^0 (top) and as a function of the proper lifetime for four values of the mass (bottom). The bottom plot also shows the expected upper limits with one standard deviation uncertainties.

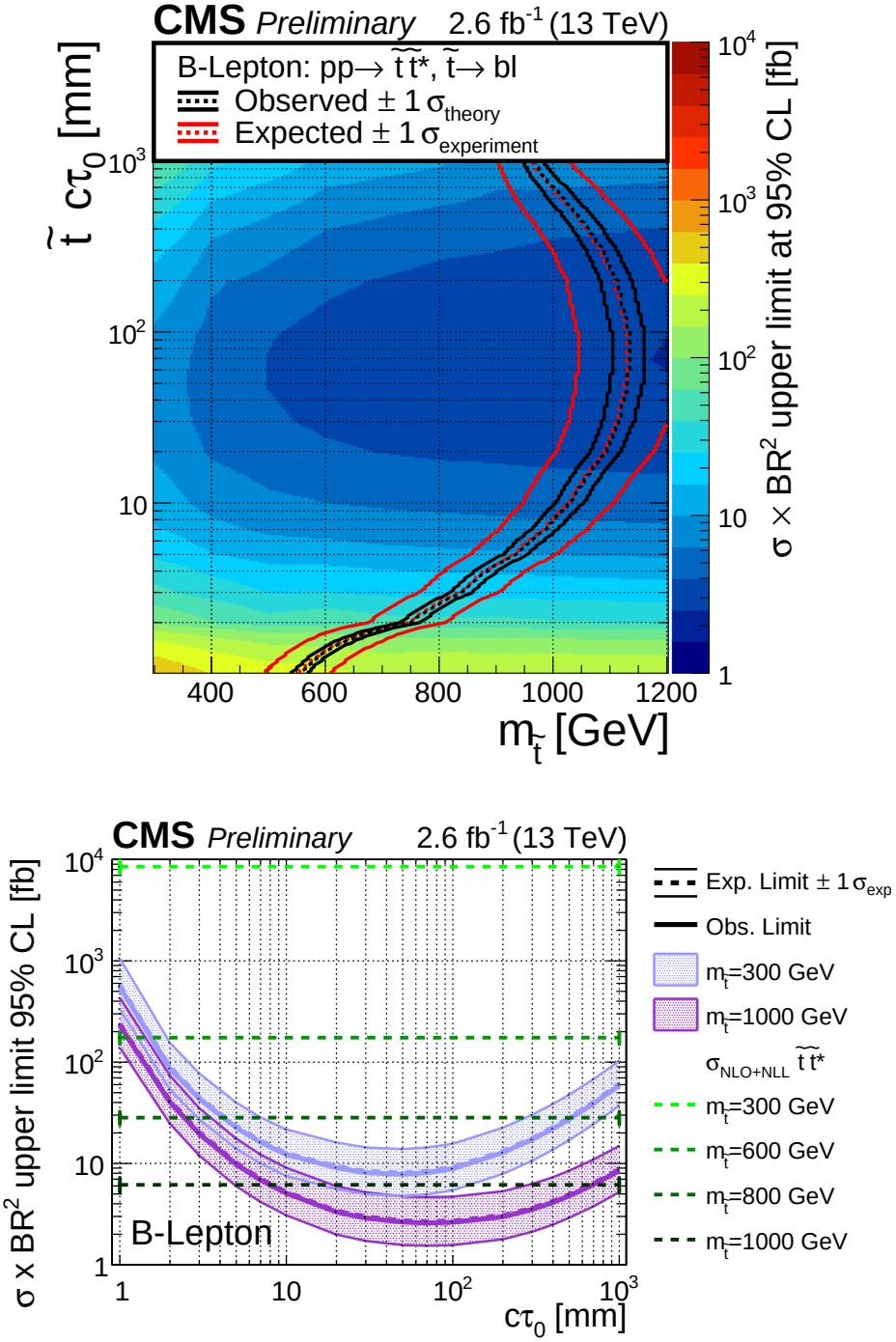

Figure 5: The excluded cross section at 95% CL for the B-Lepton model as a function of the mass and proper lifetime of the parent particle $\tilde{t}$ (top) and as a function of the proper lifetime for two values of the mass (bottom). The top plot also shows the expected (observed) exclusion region with one standard deviation experimental (theoretical) uncertainties, utilizing a NLO+NLL calculation of the top squark production cross section. The bottom plot also shows the expected upper limits with one standard deviation uncertainties and the NLO+NLL calculation of the top squark production cross section at two mass values.

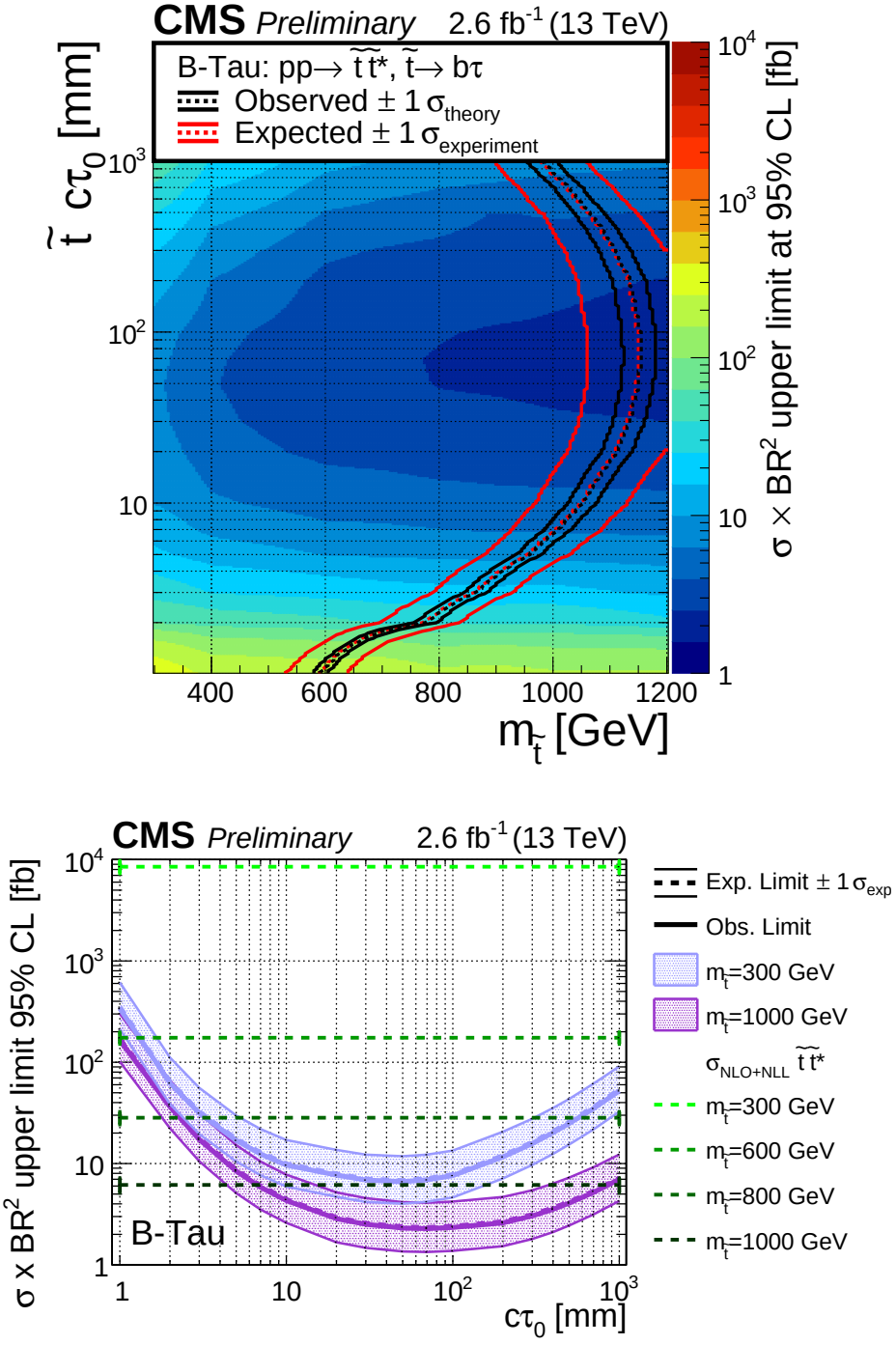

Figure 6: The excluded cross section at 95% CL for the B-Tau model as a function of the mass and proper lifetime of the parent particle $\tilde{t}$ (top) and as a function of the proper lifetime for two values of the mass (bottom). The top plot also shows the expected (observed) exclusion region with one standard deviation experimental (theoretical) uncertainties, utilizing a NLO+NLL calculation of the top squark production cross section. The bottom plot also shows the expected upper limits with one standard deviation uncertainties and the NLO+NLL calculation of the top squark production cross section at two mass values.

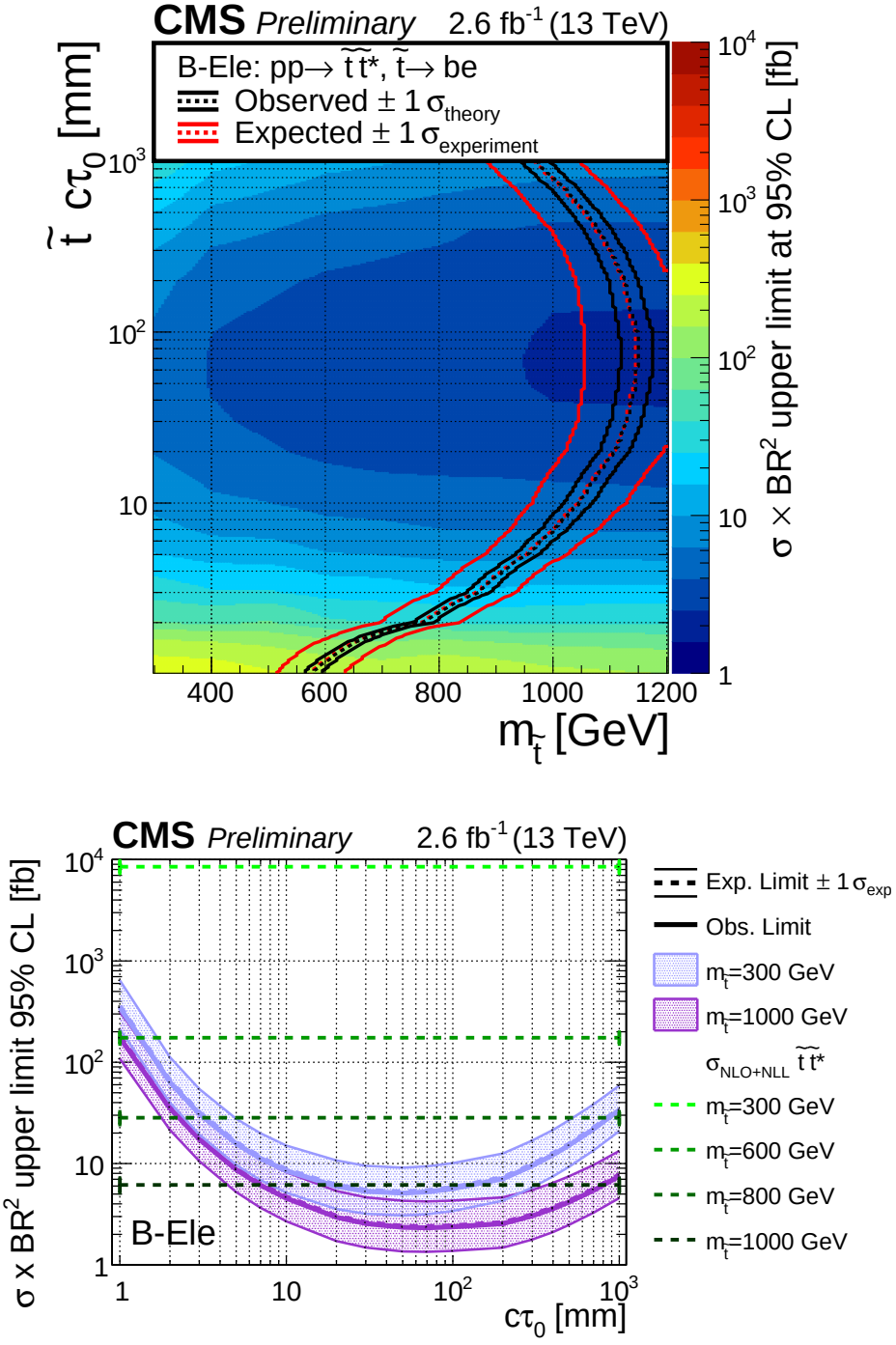

Figure 7: The excluded cross section at 95% CL for the B-Ele model as a function of the mass and proper lifetime of the parent particle $\tilde{t}$ (top) and as a function of the proper lifetime for two values of the mass (bottom). The top plot also shows the expected (observed) exclusion region with one standard deviation experimental (theoretical) uncertainties, utilizing a NLO+NLL calculation of the top squark production cross section. The bottom plot also shows the expected upper limits with one standard deviation uncertainties and the NLO+NLL calculation of the top squark production cross section at two mass values.

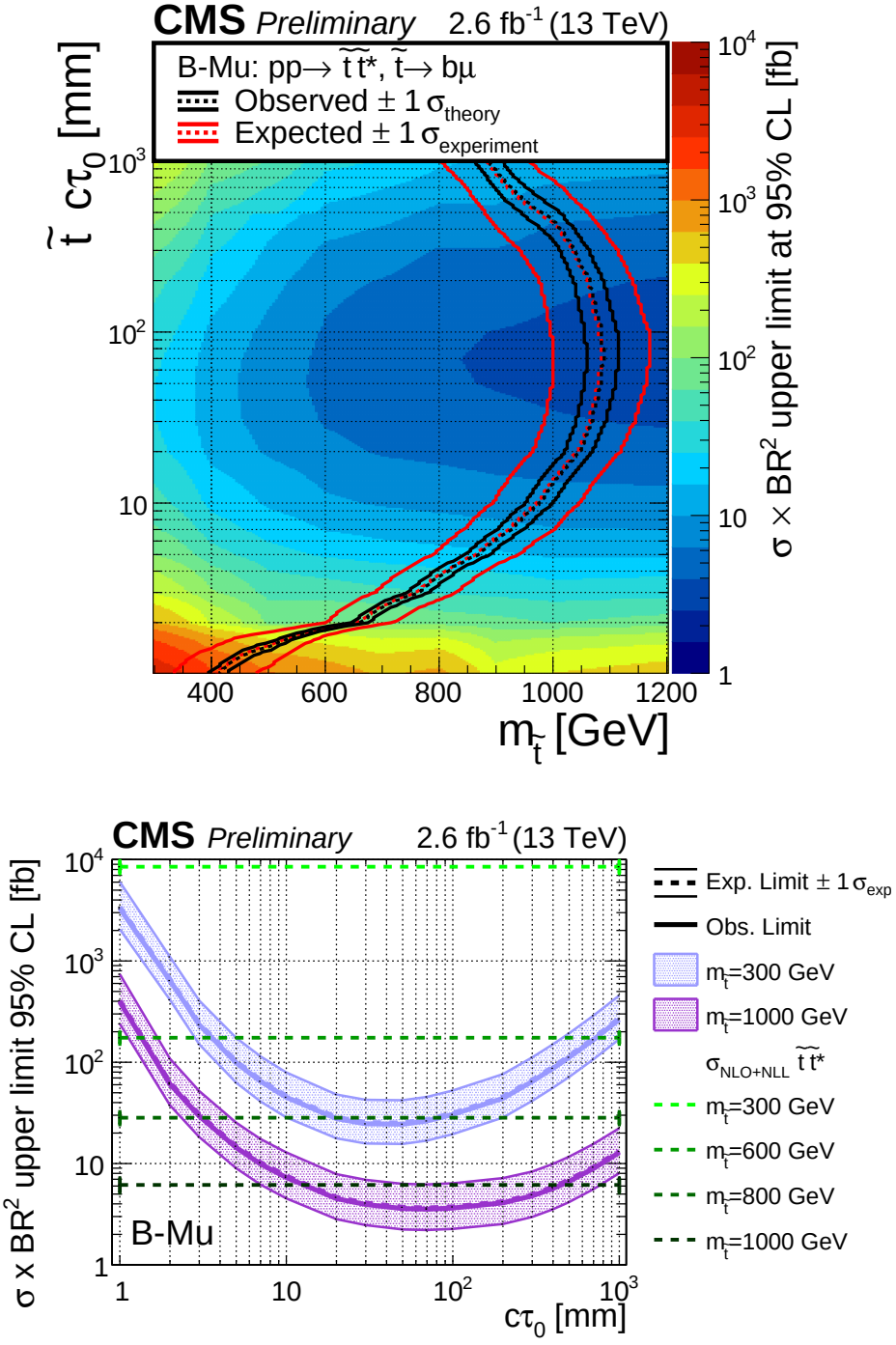

Figure 8: The excluded cross section at 95% CL for the B-Mu model as a function of the mass and proper lifetime of the parent particle $\tilde{t}$ (top) and as a function of the proper lifetime for two values of the mass (bottom). The top plot also shows the expected (observed) exclusion region with one standard deviation experimental (theoretical) uncertainties, utilizing a NLO+NLL calculation of the top squark production cross section. The bottom plot also shows the expected upper limits with one standard deviation uncertainties and the NLO+NLL calculation of the top squark production cross section at two mass values.

[3] CMS Collaboration, "Search for Long-Lived Neutral Particles Decaying to Quark-Antiquark Pairs in Proton-Proton Collisions at $\sqrt{s} = 8$ TeV", *Phys. Rev. D* **91** (2015) 012007, doi:10.1103/PhysRevD.91.012007, arXiv:1411.6530.

[4] T. Sjöstrand, S. Mrenna, and P. Z. Skands, "A brief introduction to PYTHIA 8.1", *Comput. Phys. Commun.* **178** (2008) 852, doi:10.1016/j.cpc.2008.01.036, arXiv:0710.3820.

[5] R. Ball et al., "Parton distributions with LHC data", *Nucl. Phys. B* **867** (2013) 244, doi:10.1016/j.nuclphysb.2012.10.003, arXiv:1207.1303.

[6] M. Strassler and K. Zurek, "Discovering the Higgs through highly-displaced vertices", *Phys. Lett. B* **263** (2008) 2, doi:10.1016/j.physletb.2008.02.008.

[7] P. W. Graham, D. E. Kaplan, S. Rajendran, and P. Saraswat, "Displaced Supersymmetry", *JHEP* **07** (2012) 149, doi:10.1007/JHEP07(2012)149, arXiv:1204.6038.

[8] CMS Collaboration, "Description and performance of track and primary-vertex reconstruction with the CMS tracker", *JINST* **9** (2014) P10009, doi:10.1088/1748-0221/9/10/P10009, arXiv:1405.6569.

[9] CMS Collaboration, "CMS Luminosity Measurement for the 2015 Data Taking Period", Technical Report CMS-PAS-LUM-15-001, CERN, Geneva, 2016.

[10] A. L. Read, "Presentation of search results: the CL_s technique", *J. Phys. G* **28** (2002) 2693, doi:10.1088/0954-3899/28/10/313.

[11] T. Junk, "Confidence level computation for combining searches with small statistics", *Nucl. Instrum. Meth. A* **434** (1999) 435, doi:10.1016/S0168-9002(99)00498-2, arXiv:hep-ex/9902006.

[12] CMS and ATLAS Collaborations, "Procedure for the LHC Higgs boson search combination in Summer 2011", (2011). CMS-NOTE-2011-005.

[13] W. Beenakker, R. Höpker, M. Spira, and P. M. Zerwas, "Squark and gluino production at hadron colliders", *Nucl. Phys. B* **492** (1997) 51, doi:10.1016/S0550-3213(97)80027-2, arXiv:hep-ph/9610490.

[14] A. Kulesza and L. Motyka, "Threshold resummation for squark-antisquark and gluino-pair production at the LHC", *Phys. Rev. Lett.* **102** (2009) 111802, doi:10.1103/PhysRevLett.102.111802, arXiv:0807.2405.

[15] A. Kulesza and L. Motyka, "Soft gluon resummation for the production of gluino-gluino and squark-antisquark pairs at the LHC", *Phys. Rev. D* **80** (2009) 095004, doi:10.1103/PhysRevD.80.095004, arXiv:0905.4749.

[16] W. Beenakker et al., "Soft-gluon resummation for squark and gluino hadroproduction", *JHEP* **12** (2009) 041, doi:10.1088/1126-6708/2009/12/041, arXiv:0909.4418.

[17] W. Beenakker et al., "Squark and gluino hadroproduction", *Int. J. Mod. Phys. A* **26** (2011) 2637, doi:10.1142/S0217751X11053560, arXiv:1105.1110.

[18] M. Krämer et al., "Supersymmetry production cross sections in pp collisions at $\sqrt{s} = 7$ TeV", (2012). arXiv:1206.2892.